Biomaterials 148 (2017) 54–68

Contents lists available at ScienceDirect

Biomaterials

journal homepage: www.elsevier.com/locate/biomaterials

In situ sequestration of endogenous PDGF-BB with an ECM-mimetic sponge for accelerated wound healing

Qiu Li [a], Yiming Niu [a], Huajia Diao [b], Lintao Wang [b], Xiuping Chen [a], Yitao Wang [a], Lei Dong [b, **], Chunming Wang [a, *]

[a] State Key Laboratory of Quality Research in Chinese Medicine, Institute of Chinese Medical Sciences, University of Macau, Macau SAR, China
[b] State Key Laboratory of Pharmaceutical Biotechnology, Nanjing University, Nanjing, 210093, China

ARTICLE INFO

Article history:
Received 21 August 2017
Received in revised form
21 September 2017
Accepted 22 September 2017
Available online 23 September 2017

Keywords:
Biomimetic scaffolds
Extracellular matrix
Polysaccharides
Growth factors
Wound healing

ABSTRACT

Recapitulating the typical features of extracellular matrix (ECM) in engineered biomaterials is crucial for preparing a suitable niche to activate endogenous tissue repair. Here, we report the design and evaluation of an ECM-mimetic scaffold that successfully accelerated wound healing through enriching endogenous platelet-derived growth factor-BB (PDGF-BB). Specifically, we prepared a electrospun hydrogel sponge (EGS) comprising a PDGF-BB-binding polysaccharide (EUP3) and gelatin. The two polymers in concert exerted a 'retention-and-release' function: upon the application of EGS *in vivo*, EUP3 started to bind and sequester endogenous PDGF-BB at the wound site; gradually, gelatin was degraded to free the PDGF-BB/EUP3 complex that acted on the cells *in situ*. Our serial *in vitro* and *in vivo* tests validated the efficacy of EGS in retaining PDGF-BB, releasing PDGF-BB/EUP3 in response to collagenase, and promoting various PDGF-BB-mediated regenerative activities. Particularly, EGS accelerated the repair of a full-thickness skin wound in mice and induced optimal neo-tissue formation, without the addition of any exogenous GFs, cells or genes. Collectively, our results suggest that, by mimicking the distinctive GF-affinitive feature of ECM, EGS as an engineered biomaterial can effectively harness the endogenous regenerative power of the native tissue. Our investigation may inspire the design of new, effective and safer approaches for tissue regeneration.

1. Introduction

Design of biomaterials for wound healing and tissue regeneration aims to restore the physical and biological functions of extracellular matrix (ECM), which is the natural scaffold of tissue cells [1–4]. In addition to its fundamental roles in supporting cell growth and guiding tissue formation [5–7], one distinctive feature of ECM is its affinity for numerous growth factors (GFs) that are key biological mediators of the healing process [8–10]. Like a sponge, ECM absorbs GFs in its three-dimensional (3D) network; but beyond physical absorption, ECM can further retain the GFs through affinitive bindings – between its certain polysaccharide components called glycosaminoglycans (GAGs) and specific domains on the GFs [4,11,12]. These bindings protect the GFs from degradation, enrich their local concentration and enable them to interact with cellular receptors [13–15]. Thus, establishing proper binding of GFs to a matrix is an essential pre-requisite for GFs to exert their biological actions [12,16,17].

Nevertheless, few current biomaterials scaffolds could recapitulate this prominent feature of ECM. Engraftment of these scaffolds could hardly enrich endogenous GFs (which are usually secreted more abundantly than normal and accumulate in response to injury) or protect exogenous ones (which are often delivered in an excessive amount to the wound bed [18,19]). Consequently, GFs that are in high demand either diffuse or degrade rapidly, failing to activate the tissue's endogenous healing potential and orchestrate the regenerative process. Meanwhile, overdosing is often required and causes severe safety concerns [20–22]. It emerges as a pressing need to devise a scaffold that can mimic ECM in sequestering the endogenous, pro-regenerative GFs around the site of injury and thereby create a suitable niche to facilitate endogenously-driven tissue regeneration.

Our recent discovery of a galacturonic acid-containing polysaccharide with unique GF-binding affinity may provide inspiration

* Corresponding author.
** Corresponding author.
E-mail addresses: leidong@nju.edu.cn (L. Dong), cmwang@umac.mo (C. Wang).

https://doi.org/10.1016/j.biomaterials.2017.09.028
0142-9612/

[23]. This polysaccharide, namely EUP3, demonstrated an extraordinary bioactivity among natural polymers – it could preferentially bind platelet-derived growth factor-BB (PDGF-BB) and specifically enhance the latter's function both *in vitro* and *in vivo* [23]. EUP3 possesses desirable properties as the material to fabricate a GF-affinitive scaffold. First, it selectively facilitates the action of PDGF-BB. This potent mitogen plays a pivotal role in almost every stage of wound healing; but it has an exceptionally short half-life in the wound fluid [24–28] and requires binding to ECM (or possibly an ECM-mimetic scaffold) [29,30]. Second, except for strengthening the action of PDGF-BB, EUP3 exerted no bioactivity (and thus side effect) on its own. It has no sulphate groups and is not derived from animals, thereby avoiding undesirable activities commonly found with molecules with such properties [31–35]. Third, as a polysaccharide macromolecule, EUP3 has an adequate size to be incorporated into polymer network without easy leakage.

Although EUP3 can be used to fabricate a scaffold to bind PDGF-BB, a further challenge emerged: how could this scaffold enrich PDGF-BB in its framework while enabling the GF to act on the cells around the injury site? Physiologically, ECM solves this issue by adjusting the concentration gradients of GFs in a highly dynamic and sophisticated manner [36]. Here, we devised a 'retention-and-release' mechanism to achieve the goal. We selected EUP3 and gelatin as the building blocks of the scaffold. Gelatin, an FDA-approved natural polymer, has two roles in our design. First, it supports cell adhesion [37,38], which fulfils the fundamental role of ECM. Second, it is a substrate of type IV collagenase [39], which is produced in elevated levels by keratinocytes and other cells involved in the healing of the skin [40,41]. We expected that – soon after scaffold implantation, EUP3 starts to bind and sequester the endogenously produced PDGF-BB into the scaffold ('retention'). As healing continues, cells secrete more collagenase to degrade gelatin, freeing the molecular complexes of EUP3/PDGF-BB that further act on the cells ('release'). We hypothesised that scaffolds with such a local, retention-and-release control of PDGF-BB could activate the body's endogenous regenerative power for wound healing, without the addition of exogenous GFs or other therapeutic agents (Scheme 1). To validate our hypothesis, we first employed the electrospinning technology to fabricate EUP3 and gelatin into a fibrous scaffold, mimicking the microstructure of the skin tissue ECM [42,43]. Then, we evaluated its effects in sequestering endogenous PDGF-BB and enhancing the function of this GF in various aspects – specifically in promoting cell proliferation, inducing neovascularisation and eventually accelerating wound healing in mice created with full-thickness wounds.

2. Materials and methods

2.1. Electrospinning fabrication of EUP3/gelatin fibres

The EUP3 polysaccharide, which we discovered and reported for the first time, was routinely isolated from *Eucommia ulmoides Oliv* and characterised in our laboratory according to our published protocol [23]. The proposed structure of EUP3 is shown in Fig. S1. Gelatin (porcine skin, type-A powder, Sigma; 120 mg) and EUP3 (20 mg) was dissolved in trifluoroethanol (TFE, Aladdin, China; 1 mL) and ddH_2O (1 mL), respectively. The two solutions were mixed to ensure the ratio of EUP3 to gelatin to be 1:36, 1:16, 1:6 and 1:4 (w/w). The mixture was filled into a syringe and kept in a syringe pump attached with the electrospinning instrument (Tongli Weina, China). The fibres were collected with an aluminium foil collector plate (10 × 10 cm). The distance between the syringe and the collector was set at 13 cm, with a 15 kV voltage and flow rate of 1 mL/h.

The obtained fibres were crosslinked into scaffolds by using the glutaraldehyde vapour (0.25%, w/v) for 30 min at room temperature, followed by washing with 1 M glycine aqueous solution to block the unreacted glutaraldehyde. The scaffolds prepared from pure gelatin were numbered as Sample I and referred to as GS, and those with a EUP3/gelatin proportion of 1:36, 1:16, 1:6 and 1:4 were numbered as Samples II to V, respectively. Sample IV was referred to as EGS in most experiments.

2.2. Characterisation of the fibres and scaffolds

The morphology of the fibres/scaffolds was observed by scanning electron microscope (FEI nanoSEM 430, USA). The average diameter was calculated using ImageJ, with at least 100 different fibres collected from each image. The porosity of the scaffolds was calculated by densimetry and each value was obtained from six repeated measurements [44]. To visualise EUP3 in the scaffolds, this polysaccharide was labelled with fluorescein-5-thiosemicarbazide (FTSC), by reacting with FTSC (EUP3: FTSC = 10: 1, W/W) for overnight at room temperature in the presence of 1-Ethyl-3-(3-dimethylaminopropyl)-carbodiimide (EDC) and N-hydroxysuccinimide (NHS) in MES solution (EUP3/EDC/NHS = 3:3:1, w/w/w, pH = 5.0) [45]. After weaving into the fibres and crosslinking into scaffolds, the fluorescence signal was detected by using a fluorescent microscope (IX73, Olympus).

The tensile strength and air permeability of the fibres/scaffolds were measured by Instron 5848 (Instron, Canton, MA) and the air permeability tester (PORTAIR FX3360, Switzerland), respectively. The contact angles of the scaffolds were continuously measured within 10 s by five-point fitting method with a contact angle instrument (JC-2000D1, Powereach Co.). The thermal stability of the scaffolds was measured by the TGA technology (TGA/DSC1, METTLER TOLEDO). The samples were weighted in open aluminium pans and heated from 25 to 800 °C with the rate of 10 °C/min. In addition, the water retention of the samples was measured. Briefly, the weight of the samples before and after 24-h water absorption was defined as w_d and w_0, respectively. The samples were then left in air at room temperature and the weight (w_t) was measured at pre-determined time points. The water sorption was calculated according to the following equation.

$$SR = \frac{w_t - w_d}{w_d} \times 100\%$$

2.3. Determination of VEGF-A, FGF-2 and PDGF-BB bound to the sponges

The amount of murine VEGF-A, FGF-2 and PDGF-BB (Peprotech, USA) sequestered by the sponges was determined by ELISA. Different sponge samples were incubated with recombinant VEGF-A, FGF-2 and PDGF-BB (10 μg/mL in PBS) in 24-well plates for overnight at 4 °C. After proper rinsing against PBS to remove the unbound GFs, the samples were homogenised in PBS, vortexed (1 min) and centrifuged (10,000 rpm; 5 min). The supernatants were carefully aliquoted and measured using corresponding ELISA kits (R&D systems, USA). Additionally, the presence of PDGF-BB retained by the sponges were visualised *in situ* by using a modified ELISA protocol, by incubating the substrates with anti-PDGF-BB, rinsing and directly staining.

2.4. Cell adhesion, proliferation and GF-retention in vitro

The mouse fibroblast cell line NIH-3T3 (ATCC, USA) was cultured in Dulbecco's Modified Eagle Medium (DMEM) with the addition of

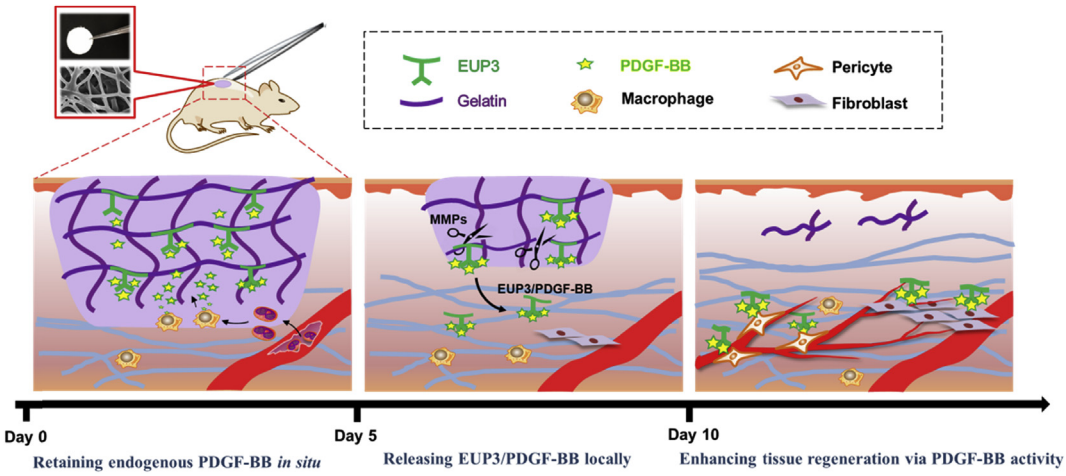

Scheme 1. Schematic illustration of the mechanisms of the designed ECM-mimetic sponge (EGS) for wound healing. EGS, with its unique PDGF-BB-binding affinity and collagenase-responsive degradability, exerted to harness the regenerative activity of the endogenous PDGF-BB for accelerating wound healing *in situ*. Inset images on the top left: a gross view and SEM observation of the fibrous scaffolds of EGS.

10% FBS. The cells were seeded onto EGS or GS sponges with or without pre-incubation with PDGF-BB (5×10^4/sample) and incubated at 37 °C for 24 h. First, the viability and gross morphology of the cells were examined by calcein-AM staining (15 min) and observation under a confocal microscope (Nikon, Japan). Second, following proper rinsing with PBS, the cells were fixed with glutaraldehyde (2.5%) for overnight at 4 °C, followed by dehydration with a gradient of ethanol solutions (from 30% to 100%), freeze-drying and gold coating for SEM observation.

Third, the cell viability was quantitatively measured by with a CCK-8 assay at day 1 and 3. To each mL of cultural medium, one hundred microliter of CCK-8 agent was added to each well and incubated for 2 h at 37 °C. Then, 100 μL of the final medium was transferred into the 96-well plate and the absorbance was measured at 450 nm on a microplate reader.

Fourth, the retention of PDGF-BB *in vitro* was assessed by immunofluorescent (IF) staining. As described above, the cells treated for 24 h were fixed with paraformaldehyde (4%; 20 min), blocked with BSA (5%; 30 min) and incubated with the primary antibody (anti-PDGF-BB, Bioss Technology, China) for overnight at 4 °C. After proper rinsing against sterile PBS, incubation with a secondary antibody (AlexaFluor488-conjugated anti-rabbit, Cell Signaling Technology, USA) and counter-staining with DAPI, the cells were observed under a confocal microscope.

2.5. Western blotting (WB)

As described before, the cells were seeded onto the sponges with or without pre-incubation with PDGF-BB. After incubation for 24 h at 37 °C, the cells were gently rinsed with cold PBS and lysed with RIPA buffer containing protease. The lysate was collected and centrifuged (rpm 14,000 g, 15 min) to obtain total proteins, which were then quantified (MicroBCA Kit, Thermo Scientific, USA) and subjected to WB. Briefly, equal amounts of protein samples were resolved with SDS-PAGE electrophoresis and transferred to PVDF membranes (Bio-Rad, USA). The membranes were then blocked with skimmed milk or bovine serum albumin (5%) for 1 h at room temperature with gentle shaking, blotted with anti-PDGFR (1:1000, Cell Signalling, USA) at 4 °C for overnight and incubated with secondary antibody for 2 h at room temperature. The bands were visualised with the SuperSignal West Pico Chemiluminescent Substrate (Thermo Scientific, USA).

2.6. Degradation

The scaffolds of EGS or GS were cut into pieces, seeded into 24-well plates and incubated at 37 °C in collagenase IV (0.5 mL/well, 0.8 units/mL of PBS) or PBS as control. The solution was changed every other day. The samples were collected by centrifugation and rinsed for three times against ddH_2O, followed by lyophilisation and measurement of the mass. Additionally, the fibres collected at day 3 and 7 were observed by SEM.

2.7. The releasing profile of PDGF-BB

To sketch the release profile of PDGF-BB from the sponges, the PDGF-BB-incubated samples were placed in PBS (pH 7.4; 1 mL) or collagenase IV solution (1 mL, 0.8 units/mL of PBS) and kept on a shaker at 37 °C. The GF released from the sponges was collected at different time points (from day 1 to day 12), with fresh PBS or collagenase IV solution replenished. The amount of PDGF-BB was assayed using ELISA.

2.8. Gel-shift and co-immunoprecipitation (co-IP) assays

EGS/GS incubated with PDGF-BB (and rinsed gently) were put in the transwell membrane inserts (Corning Inc., NY, USA) placed into the 24-well tissue culture plates. Collagenase IV (200 μL; 0.8 units/mL of PBS) and PBS (600 μL) were added into the upper transwell insert and the lower chamber, respectively. The sponges were incubated at 37 °C for 72 h, with the solution in the lower chamber collected, stored at −80 °C and replenished with fresh PBS every 12 h. Each collected sample was lyophilised and separately re-dissolved in PBS (10 μL) for the subsequent experiments.

The gel shift assay was performed by native polyacrylamide gel electrophoresis [46]. Briefly, the above solution was loaded onto a native polyacrylamide gel (T (%) = 12%,T (%) = [acrylamide + bis-acrylamide/V (mL)] × 100%; C (%) = 3.3%; C (%) = bis/(acr + bis) × 100%; separating buffer was 0.06 M potassium hydroxide, pH 4.3). The loading buffer consisted of 15% glycerol, 0.02% methyl green and 70 mM β-alanine. The running buffer was 0.14 M β-alanine (pH 4.5). Electrophoresis was performed under 70 V on ice for 1 h followed by Coomassie Blue Fast Staining Solution (Beyotime, China).

The co-IP experiment was performed according to an established protocol [14]. Briefly, the acquired solution was incubated

with or without PDGFRβ Fc chimera (500 ng/mL, R&D Systems, USA) at room temperature for 2 h. The complex was precipitated with the Protein A/G Agarose (Santa Cruz Biotechnology, USA) for 10 h at 4 °C. The solution was centrifuged (10,000 rpm, 15 min) and the supernatant discarded. The acquired samples were subjected to the phenol-sulfuric acid assay to detect the presence of sugars and the absorbance was measured at 490 nm. Meanwhile, according to the standard protocol, the acquired solution was eluted with equal and adequate PAGE sample buffer containing 1 mM phenylmethanesulfonyl fluoride (PMSF) (Sigma-Aldrich). After heat denaturation at 95 °C for 5 min and centrifugation at 12,000 rpm for 5 min, the eluted proteins were loaded onto the SDS-PAGE gel for WB examination with anti-PDGF-BB (1:2000, Abcam, UK). Both the input control and isotype control (Mouse IgG; 500 ng/mL, ThermoFisher Scientific, USA) were set for the IP experiment.

Moreover, the obtained solution was incubated in equal volume with maximum recovery diluent (MRD, Thermo Scientific, USA, diluted with PBS in equal volume) that mimic the wound bed microenvironment [47], and the activity of PDGF-BB was measured by ELISA. Further, we seeded the fibroblasts onto the bottom of the Transwell device, and placed EGS/GS pre-incubated with PDGF-BB (following rinsing) in the upper inserts with the addition of collagenase IV as described before. Cell proliferation was determined with a CCK-8 assay at different time points.

2.9. Full-thickness wound model

The animal protocols were approved by the Animal Care and Use Committee of Nanjing University and conformed to the Guidelines for the Care and Use of Laboratory Animals published by the National Institutes of Health. C57BL/6 mice (male, 18–20 g) were provided by the Experimental Animal Centre of Nanjing Medical University (Nanjing, China). A total of 30 male mice, weighing between 18 and 20 g, were anesthetised and cut off with one circular full-thickness skin wound (7 mm diameter) under the sterile conditions. The mice were randomly divided into three groups: i) blank control (no treatment except for sterile gauze), ii) receiving GS and iii) receiving EGS. The mice having recovered from anaesthesia were reared in different cages.

2.10. Analysis of wound healing

The gross view of wound was observed at 0, 3, 5, 7, 10 and 12 days after operation. The wound healing rate of different groups was calculated based on comparison with the original area of wound. In each group, wounds were excised with a 5 mm surrounding intact tissue. The tissues were immersed into the paraformaldehyde (4%) for 24 h and then embedded into paraffin. After the paraffin was sectioned, hematoxylin-eosin (H&E) and Masson's trichrome staining were carried out for histological analysis.

2.11. Retention of PDGF-BB in vivo

To evaluate the retention of endogenous PDGF-BB *in situ* and *in vivo*, the sponges were retrieved from the wounds at different days after implantation. The sponges were homogenised in PBS (pH 7.4) and centrifuged (10,000 rpm, 5 min). The supernatant was collected for the determination of PDGF-BB by ELISA. The tissue paraffin sections at the different time points were also prepared for IF staining for PDGF-BB.

2.12. Immunofluorescent (IF) staining of the tissue samples

IF staining was performed to detect the presence of PDGF-BB *in situ* as well as the expression of various specific markers. The primary antibodies (all diluted in 1% BSA) detecting murine proteins used in this study are below: anti-PDGF-BB (Bioss China, 1:200), anti-Ki67 (1:100, Abclonal Technology, China; proliferative marker), anti-CD31 (1:20, Abcam, Cambridge, UK; endothelial marker) anti-alpha-smooth actin (α-SMA, 1:200, Boster Biotechnology, China), anti-Desmin (1:200, Abcam, Cambridge, UK; both pericyte marker), anti-CD68 (1:100, Abclonal, China; macrophage/monocyte marker) and anti-CD206 (1:500, Abcam, Cambridge, UK; M2-macrophage marker). The secondary antibodies used included Alexa Flour 488-conjugated donkey-*anti*-mouse and Alexa Fluor 546-conjugated donkey-*anti*-rabbit (1: 200, Life Technologies, USA; both diluted in 1% BSA).

The paraffin sections representing samples collected at different time points were deparaffinised with xylene and ethanol, rehydrated, operated with antigen retrieval, blocked with BSA (5%, 30 min) and applied with the specific primary antibody for overnight at 4 °C. After proper rinsing against PBS, the samples were incubated with corresponding secondary antibodies and counterstained with diamidino-phenyl-indole (DAPI; Sigma-Aldrich). All images were captured on a Nikon confocal microscope (C2+, Nikon, Japan) and analysed by using the Nis-element advanced research software (Nikon).

In addition, EUP3 conjugated with the sulfo-cyanine3 carboxylic acid [48] was fabricated into EGS, for the assessment of the degradation of EGS and the binding of PDGF-BB *in vivo* (with IF staining for PDGF-BB). In certain samples, the density of microvessels was calculated and their numbers were counted in the representative areas with vascularisation, with at least three different regions randomly chosen.

2.13. Blood coagulation and biochemical analysis

The serum of mice at day 10 after operation were collected and stored at −80 °C until analysis, in which the levels of creatine kinase (CK), lactate dehydrogenase (LDH), blood urea nitrogen (BUN), aspartate transaminase (AST) and alanine aminotransferase (ALT) were assessed with corresponding kits (Jiancheng Biotech, China). The blood of mice at day 3 and day 10 after operation were collected into blood collection tubes with K_2EDTA and prothrombin time (PT) was measured with the Sysmex cs-5100 (Japan).

2.14. Statistics

For all the quantitative measurements, at least three biological replicates were performed. Data are presented as mean ± standard deviation (SD). Statistical analyses were performed using one-way ANOVA (GraphPad Prism 6), with * and ** standing for $p < 0.05$ and < 0.01, respectively.

3. Results and discussion

3.1. Preparation and characterisation of EUP3/Gelatin sponge (EGS)

We prepared EGS in two stages – i) fabricating fibres by electrospinning and ii) crosslinking the fibres into scaffolds that rapidly turned into sponges in an aqueous solution.

In the first stage, we optimised the proportion of gelatin and EUP3, with an aim to incorporate as much EUP3 as possible while ensuring the viscosity of the mixture suitable for electrospinning. Among the five sample groups, Sample I was based on pure gelatin; Sample II-V contained EUP3 and gelatin at ratios of 1:36, 1:16, 1:6 and 1:4, respectively. The spinning process of Samples I to IV went smoothly, but that of Sample V was frequently discontinuous. SEM examination showed that the diameter of the fibres ranged between 0.6 and 1 μm (Fig. 1a and Fig. S2). The porosity of the fibres

ranged from ~62% (Samples I) to ~ 68% (Samples IV). Observation of the FTSC-labelled EUP3 revealed a homogenous distribution of EUP3 in the fibres (inset images, Fig. 1a). From Sample I to IV, fibres containing increasing amounts of EUP3 showed higher fluorescent intensity and smaller average diameters; but in Sample V the fibres appeared irregular in morphology and contained knots of varying sizes. This phenomenon, together with its intermittent spinning process, suggested that the concentration of EUP3 in Sample V was too high, making the viscosity of the mixture solution too low to produce a continuous fibre.

In Samples II to IV, EUP3 demonstrated its advantage as a macromolecule component: it served as a building block of the fibres and stably embedded even without crosslinking. In contrast, when heparin, another polysaccharide with smaller molecular masses, replaced EUP3 for electrospinning, it easily leaked from the fibres between 24 and 48 h (Fig. S3). A thermal stability analysis confirmed that these fibres exhibited a similar profile, showing little change at between 50 and 80 °C but considerable weight loss at between 250 and 300 °C (Fig. 1c).

In the second stage, we crosslinked the fabricated fibres with glutaraldehyde vapour (0.25%, w/v) for 30 min into scaffolds, which exhibited a porous microstructure (Fig. 1b) and a white, opaque, fabric morphology (inset images, Fig. 1b). Samples containing more EUP3 demonstrated higher air permeability: for instance, Sample I and IV had an average permeability of 30 and 90 $cm^3/cm^2/s$, respectively (Fig. 1d). We suspected that the addition of the polysaccharide increased the porosity and thereby air permeability of the scaffolds, which could potentially benefit healing. In addition, we confirmed 30 min to be an optimal crosslinking time, as the crosslinked scaffolds quickly absorbed PBS and turned into transparent sponges within a minute. In contrast, scaffolds crosslinked for shorter than 20 min failed to form a shape in PBS, yet those crosslinked for 60 min tended to produce rigid scaffolds lacking water-absorbing capacity (Fig. 1e).

We characterised the physical properties of these five scaffolds in two aspects – i) the rate and capacity of water absorption and ii) mechanical strength. All the samples absorbed water fast – the instant contact angle (ICA) of the scaffold surface against a drop of PBS sharply decreased from 100° ± 20° to almost 0° in 5–7 s (Fig. 1f). Meanwhile, all the scaffolds absorbed PBS in the capacity of 500–550% – and retained approximately 450% after 5 days – of their own mass (Fig. 1g). As time increased, the scaffolds were gradually saturated with PBS. Additionally, the fully-hydrated scaffolds displayed typical stress-strain curves. Increasing the EUP3 ratio considerably decreased the tensile strength and elongation. For example, Sample I and IV encountered fracture at the elongation of 60% and 50% (Fig. S4a) and had Young's modulus of ~520 and ~230 kPa (Fig. S4b), respectively. We suspected that the samples with higher contents of EUP3 might have fewer crosslinks between gelatin molecules, making the scaffolds more flexible.

In summary, we have optimised the conditions to fabricate EGS and characterised the samples in different forms – fibres, scaffolds and sponges. The EUP3-containing Samples II to IV demonstrated homogenous morphology, stability and reasonable physical characteristics for wound dressings and tissue scaffolds. These data provided essential information for selecting an optimal condition to fabricate EGS as well as understanding the physical features of the materials in their various forms.

3.2. In vitro retention of VEGF-A, FGF-2 and PDGF-BB in EGS

Based on the above physical characterisation, we continued to examine the GF-retaining capacity of the different sponges by incubating them in PBS containing recombinant growth factors for 12 h. After proper rinsing, the amount of VEGF-A, FGF-2 and PDGF-BB retained in each scaffold was determined by ELISA. These samples barely absorbed VEGF-A and mildly retained FGF-2, but exhibited significantly higher binding capacity for PDGF-BB (Fig. 2a). Moreover, the samples containing higher ratios of EUP3 retained more of PDGF-BB, though there was no significant difference between the two highest samples, IV (1:6) and V (1:4), in their retained amount of PDGF-BB (Fig. 2a). These results highlighted the binding selectivity of the EUP-3-containing matrix for PDGF-BB over the other two GFs, which is consistent with our previous finding [23].

Compared with other samples, Sample IV contained a relatively high proportion of EUP3 and retained almost the highest amount of PDGF-BB; and compared with Sample V, it showed a more homogeneous fibre morphology and stable physical properties. Hence, we selected to prepare EGS in the conditions of Sample IV. Meanwhile, Sample I based on pure gelatin served as control. From this step on, the scaffolds/sponges of Sample IV and I was referred to as EGS and GS throughout this study.

We next validated the capacity of EGS and GS, in the form of sponges, in retaining PDGF-BB. By using a directly staining assay based on the principle of ELISA, we visualised the sequestration of PDGF-BB onto EGS, but not GS, after repeated rinsing in the washing buffer (Fig. S5).

Although EGS demonstrated its capability in retaining PDGF-BB, its ability to support cell growth was unknown. Thus, we examined the growth of fibroblast cells on both EGS and GS, with or without pre-incubation with PDGF-BB. First, immunofluorescent staining (IF) for PDGF-BB (green) indicated that the highest concentration of PDGF-BB accumulated on the EGS substrate pre-incubated with this GF (Fig. 2b), with the signal focused around the cell body (inset images, Fig. 2b). Second, Live staining and SEM observation illustrated that the cells adhered well on the surface of both EGS and GS sponges, showing their native spreading morphology (Fig. 2c). Among them, the cells growing on EGS supplemented with PDGF-BB had obviously the highest density and exhibited clear filopodia, which is a typical consequence of GF stimulation (inset images, Fig. 2c). Third, over 72 h, the cells proliferated faster on EGS than on GS, both supplemented with PDGF-BB (Fig. 2d). Further Western blotting analysis revealed an elevated level of phosphorylated PDGF receptor (*p*-PDGFR) in cells on EGS than those on GS – both stimulated by PDGF-BB (Fig. 2e).

We employed EUP3 to build up EGS based on its proven, selective affinity for PDGF-BB. And this polysaccharide convincingly fulfilled its mission, enabling EGS to not only retain PDGF-BB but also enhance the PDGF-mediated cellular activity. Previously, others and we explored the use of several other polysaccharides for the GF-binding purpose, notably including GAGs such as heparin/heparan sulphate (HS) [11,12,16,19,49–53]. The selection of these molecules were based on solid scientific rationale and led to valuable findings; however, they had both theoretical and technical limitations. First, heparin, the hyper-sulphated form of HS, despite being relatively easier to obtain, has severe adverse effects such as anti-coagulant/haemorrhagic and immunogenic [32,54]. Moreover, both heparin and HS lack specificity in binding GFs [53,55,56], and sophisticated technologies were needed to increase the selectivity of acquired GAGs that were already in low amounts [12,50]. In comparison, the plant-derived EUP3 molecule is obtainable in the scale of grams and with high purity, showing selective affinity and enhancing activity for PDGF-BB while possessing no immunogenicity.

3.3. In vitro release of PDGF-BB/EUP3 complex from EGS

According to our design, the PDGF-BB-retained EGS can degrade in response to type IV collagenase, which is highly expressed in the

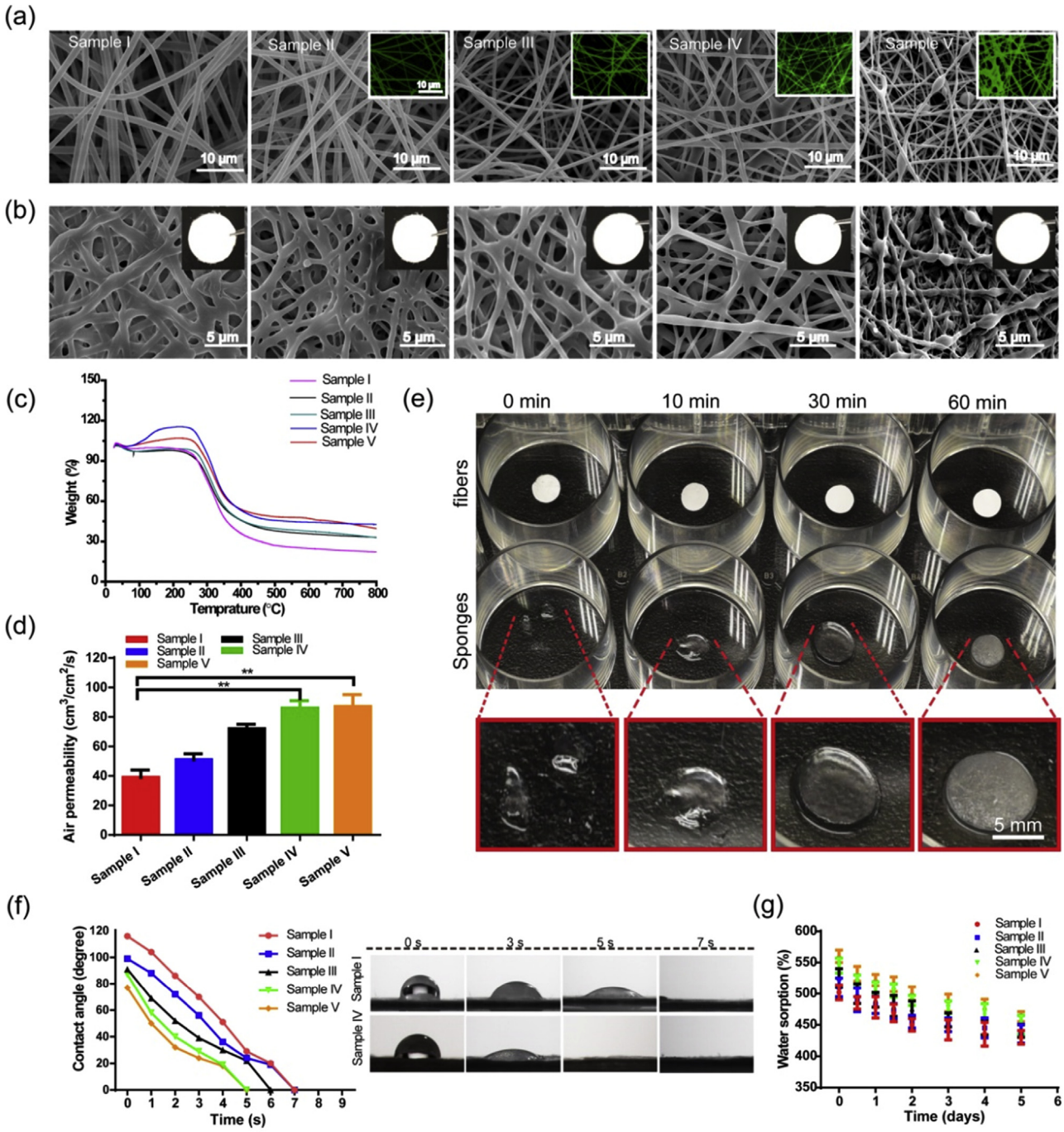

Fig. 1. Characterisation of EGS throughout the sample preparation. Sample I was based on pure gelatin; Samples II to IV contained increasing contents of EUP3: a-b) representative SEM images of a) un-crosslinked, and b) glutaraldehyde-crosslinked samples; c) TGA analysis of the samples; d) measurement of the air permeability of the samples (n = 6; $^{**}p < 0.01$); e) the morphology change from fibrous scaffolds to sponges of sample IV crosslinked for different periods of time; f) examination of the water absorption rate, as reflected by the change in instantaneous contact angle of the sponges; g) examination of water absorption capacity of the sponges.

wound bed, because its gelatin backbone is a substrate of this enzyme. We expected that this degradation would lead to the release of the EUP3/PDGF-BB complex into the microenvironment.

To verify whether type IV collagenase could trigger the degradation of the sponge, we incubated EGS and GS in PBS with or without this enzyme (0.8 units/mL of PBS). Because gelatin is a well-known degradable polymer, both EGS and GS almost entirely degraded at day 12 in PBS. However, the presence of type IV collagenase accelerated this process, causing EGS and GS to degrade completely after 6 and 8 days, respectively (Fig. 3a). SEM observation of EGS samples collected at day 3 and 7 revealed the structural change during the degradation (Fig. 3b). The degradation kinetics of EGS in the presence of the enzyme should approximately match the typical rate of neo-tissue growth and thus be favourable for wound healing.

We next assessed the ability of EGS in retaining and releasing PDGF-BB, in the absence and presence of type IV collagenase, respectively. In the absence of the enzyme, GS pre-incubated with PDGF-BB failed to hold the GF, which was almost completely released within 2 days; however, EGS retained over half amount of

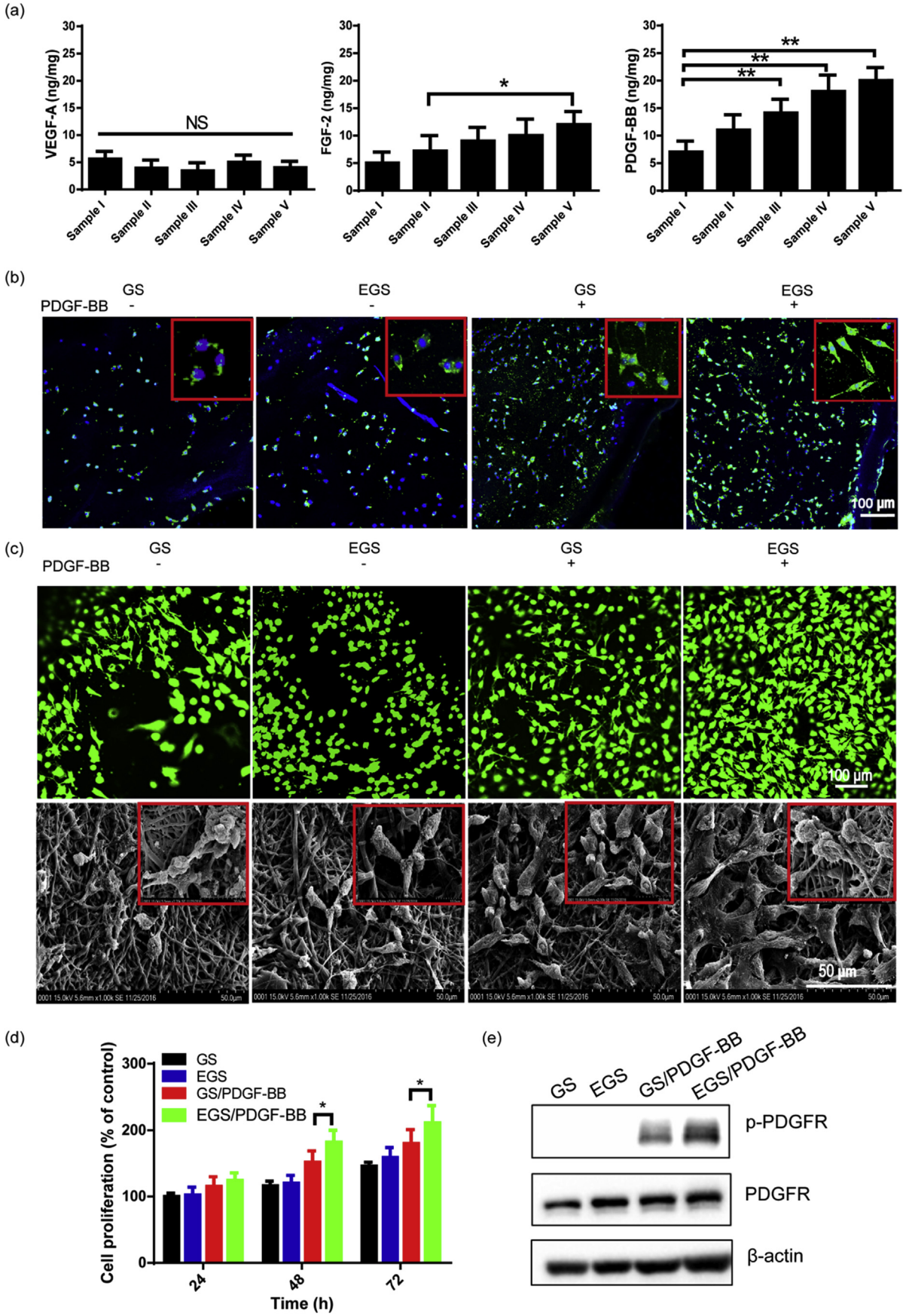

Fig. 2. *In vitro* examination of the retention of PDGF-BB by EGS: a) the amount of VEGF-A, FGF-2 and PDGF-BB sequestered by the different samples (n = 6; $^{**}p < 0.01$); b) representative images of immunofluorescent staining for PDGF-BB retained by EGS and GS; c) representative images of Live staining assay and SEM observation for fibroblasts on EGS and GS, pre-treated or not with PDGF-BB; d) cell proliferation and e) the activation of PDGFR signalling pathway in the cells cultured on EGS and GS, pre-treated or not with PDGF-BB.

PDGF-BB at 5 days (Fig. 3c). In the presence of the collagenase, the release of PDGF-BB from the EGS sponge was accelerated owing to the added enzyme and reached around 70% after 4 days; though it was likewise burst released from GS within 2 days (Fig. 3d). These data validated the expected, critical 'retention-and-release' feature of EGS, which demonstrated to retain PDGF-BB in its matrix and release it upon enzyme cleavage.

Since the collagenase cleaves gelatin but not EUP3, and since PDGF binds to EUP3 in the scaffold, we assumed that a PDGF/EUP3 complex – instead of the GF alone – was released from EGS after collagenase treatment. To validate this, we incubated the PDGF-BB-absorbed EGS in the upper insert of a Transwell device and added type IV collagenase into the insert. From the lower chamber, we collected the degraded products that could penetrate the insert membrane (Fig. 4a). A native gel electrophoresis revealed that the movement of PDGF-BB was significantly retarded, as compared with its positions in other groups (Fig. 4b). We could exclude gelatin molecules as a main influence for two reasons – i) theoretically, gelatin has no specific affinity for PDGF-BB except for some weak interactions; ii) the data showed that the band of PDGF-BB retrieved from the GS group appeared almost at the same place of the recombinant protein. Thus, the retardation should be attributed to the formation of the complex between EUP3 and PDGF-BB.

To further prove that EUP3 and PDGF-BB were complexed in the degradation product collected from EGS, we performed a co-immunoprecipitation (co-IP) assay to pull down PDGF-BB/EUP3, with the acquired solution before immunoprecipitation set as the input control and the group added with a mouse anti-IgG set as isotype control. The simultaneous presences of the polysaccharide and PDGF-BB in the EGS degradation sample were confirmed by a phenol-sulfuric acid assay (Fig. 4c) and a WB assay, respectively (Fig. 4d). The quantitative result of the phenol-sulfuric acid assay was in good agreement with the colorimetric outcome (Fig. 4e), which indicated that PDGF-BB was complexed with EUP3 when being released.

In our design, EUP3 could bind and protect PDGF-BB against degradation. To verify it, we collected the released products and added them into the MRD solution – a commercially-available, peptone-containing product that mimic the wound fluid [47]. According to the ELISA results, PDGF-BB from the 'leftover' of GS rapidly degraded, losing over 75% after 8 h; encouragingly, PDGF-BB in the EGS release products resisted degradation, with around 60% still detectable after 8 h (Fig. 4f).

We further confirmed that the released product from EGS accelerated the growth of fibroblasts. After 72 h of treatment, the viability of the cells treated with the lower-chamber solution from EGS and GS was ~2.2 and 1.6 folds of that of the untreated cells, respectively (Fig. 4g). This result suggested that binding with EUP3 amplified the mitogenic effect of PDGF-BB on these cells.

This series of findings about 'release' answered two questions crucial to our design. First, EGS (also GS) could be degraded by collagenase IV, which was the basis for the 'bio-responsive' degradation of this scaffold in the wound environment. Second, once degraded, the scaffold released PDGF-BB in the form of PDGF-BB/EUP3 complex that could exert the activity of PDGF on cells, which was pivotal for EGS to initiate the PDGF-BB-mediated regenerative actions. These data, together with the earlier findings regarding 'retention', validated *in vitro* the 'retention-and-release' function of EGS.

3.4. In vivo retention of PDGF-BB by EGS

The *in vivo* regenerative performance of EGS was evaluated in the full-thickness injury model created in mice. We first monitored the retention of endogenous PDGF-BB *in situ* to EGS, which is fundamental to its therapeutic efficacy. The outcomes from IF staining showed that PDGF-BB accumulated more in EGS than GS or control group (without any sponge) at day 3. At day 5, it not only appeared more but also penetrated deeper into the implanted EGS – but not GS. At day 10, PDGF-BB remained in a high amount and spread from the edge to the inside of the EGS implants, but almost disappeared in both control and GS groups (Fig. 5a). Determination of PDGF-BB in the implants (or in the neighbouring tissues in control) by ELISA indicated that significantly more PDGF-BB was enriched in EGS (7.9 ng PDGF per mg total protein) than in GS (5.2 ng/mg) or control (3.8 ng/mg) 3 days after implantation, and this trend maintained throughout the experiment (Fig. 5b).

To more directly observe the sequestration of endogenous PDGF-BB by EGS, we employed sulfo-cyanine3 carboxylic acid-labelled EUP3 to fabricate a batch of EGS samples for implantation and performed IF staining for PDGF-BB as described above. From the samples collected at day 5 and day 10, we could see a widespread co-localisation of the sugar and GF (Fig. 5c): at day 5, PDGF-BB tangled with EUP3 extensively as they were responding to the beginning of EGS degradation; at day 10, as the sponge further degraded and neo-tissue grew, both the molecules were more scattered and possibly interacted with the cells, but co-localisation of their signals was still apparent. These findings provided evidence of the complexation of EUP3/PDGF-BB *in situ*.

The effective retention of PDGF-BB by EGS *in vivo* was particularly encouraging because it proved our concept of using a bioactive polymer to 'enrich an endogenous GF', rather than to 'accompany the delivery of an exogenous GF' – the latter had been trialled in numerous studies using GAGs [11,16]. In mimicking how the native ECM functions in the healing process, EGS recruited and enriched the locally produced PDGF-BB in its framework, preparing a niche for PDGF-BB to exert its repairing activities. In other words, EGS served to induce, harness and fulfil the inherent regenerative potential of the target tissue, which is essentially different from conventional concepts that a scaffold is designed to protect and promote the activity of an exogenous GF delivered into the body.

3.5. In vivo enhancement of PDGF-BB activity by EGS

According to our design, EGS sequesters PDGF-BB *in situ* and enhances the functions of this GF in tissue regeneration. Although PDGF-BB plays essential and versatile roles in the multiple stages of wound healing, the two most established ones are – i) stimulate mesenchymal cells proliferation [57,58] and ii) promote blood vessel maturation [59,60]. Therefore, we investigated whether EGS could strengthen these two roles of PDGF-BB, by examining the expression of ki-67, CD31, desmin and α-SMA 5 and 10 days after implantation. The outcomes of IF staining are illustrated in Fig. 6a. First, the number of ki-67-positive cells remarkably increased in EGS at day 5, compared with the other two groups, suggesting that EGS effectively strengthened the mitogenic effect of PDGF-BB at the site of implantation. Next, the migration of endothelial cells to the site of injury was found in all these groups, which was part of the natural process of wound healing. EGS contained only mildly more CD31-positive cells than GS did. However, the key to successful revascularisation is not only the lining of endothelial cells but, more importantly, the maturation of newly formed vessels, as characterised by the recruitment of pericytes/smooth muscle cells. Then, we noticed that both desmin and α-SMA, which are markers for vasculature maturation [61], were remarkably higher in EGS than in the two other groups, particularly at day 10. And the quantitative data of the fluorescent intensity, which showed the similar trend, further confirmed the findings (Fig. S6a). Meanwhile, quantification of the density of blood vessels revealed that new blood vessels were

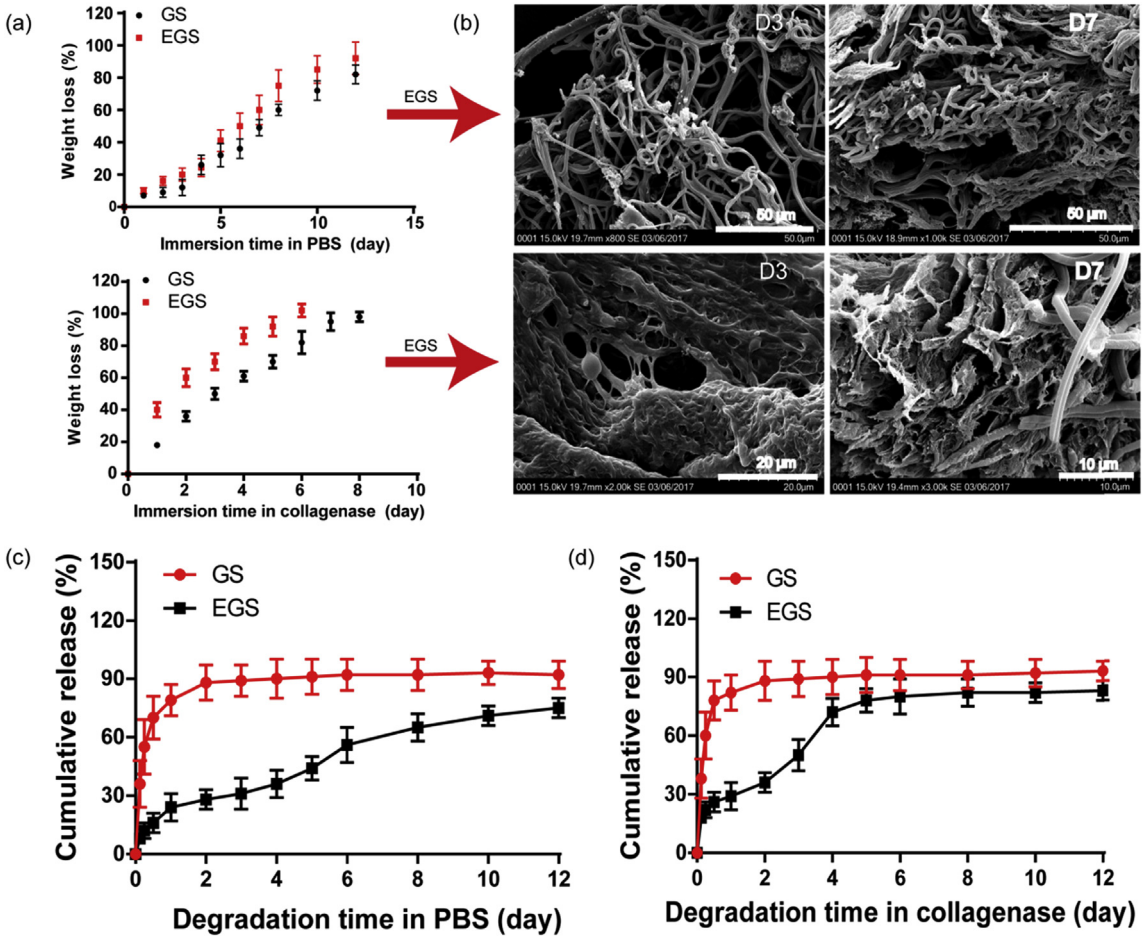

Fig. 3. *In vitro* assessment of sponge degradation and PDGF-BB release: a) the degradation profiles of EGS and GS in PBS or type IV collagenase; b) representative SEM images of EGS under degradation in PBS or type IV collagenase at day 3 and day 7; c-d) determination of PDGF-BB released from EGS or GS in c) PBS or d) type IV collagenase through 12 days.

present in the highest number in EGS among the three groups, increasing from by average 86 to 118 microvessels per hot spot at day 5 to day 10 (Fig. 6c). These data demonstrated that EGS, through sequestering endogenous PDGF-BB, could effectively enhance cell proliferation and maturation of new blood vessels.

In addition to these two classical roles, PDGF-BB could also influence the migration and phenotypes of immune cells [62,63]. Among the multiple types of immune cells, macrophages play a central role in organising physiological events relating to wound healing [28,64,65]. As such, we examined the phenotypes of macrophages in different groups 3 and 5 days after implantation. We stained for CD68 and CD206, which are typical markers of macrophages in general and those in a pro-regenerative (or 'M2') type of polarisation, respectively. At day 3, we found the presence of macrophages in all groups, which is reasonable since a macrophage-mediated inflammatory response is an integral stage of wound healing. Neither EGS nor GS triggered excessive, acute immune responses. Interestingly, at day 5, more M2 macrophages accumulated in EGS (Fig. 6b). The quantitative data in Figure S6b also showed more CD206-positive cells in EGS group (43.2%; normalised to the intensity of nuclei) than in GS (32.8%), indicating that EGS accelerated the polarisation of the recruited macrophages into a pro-regenerative phenotype.

As such, EGS demonstrated its effect in promoting PDGF-BB-mediated activities *in vivo*, including i) cell proliferation, ii) vascularisation and iii) macrophage regulation, which are all desirable for wound healing and tissue regeneration. The first two are classical functions of PDGF-BB signalling, and their establishment provided the most convincing evidence that EGS was effective in enhancing PDGF-BB-mediated regeneration *in vivo* and *in situ*. Interestingly, the third activity, though favourable, was slightly less expected. Despite several reports revealing the role of PDGF-BB on the activity of different immunocytes [63,66–68], there still lacked a link between this GF and macrophage polarisation. Also, phenotypic change of macrophages in wounds is highly dynamic and can be affected by many factors. Thus, we considered the observed change in macrophage behaviour as a positive sign and consequence of improved microenvironment, rather than attributing it to the effect of PDGF-BB or any other signalling molecule alone. To sum up, the encouraging findings in these three aspects highlighted that EGS managed to sequester PDGF-BB and support the physiological activities organised by this GF – in perfect accordance with our design.

3.6. Acceleration of wound healing by EGS

We finally examined the healing of the full-thickness wounds covered by EGS and GS, in parallel to untreated control. All the mice survived through the 12-day observation; all wounds recovered gradually without infection, with the accelerated healing observed in the EGS group only. As illustrated in Fig. 7a and quantitatively demonstrated in Fig. 7b, wound sizes measured at day 3 had no

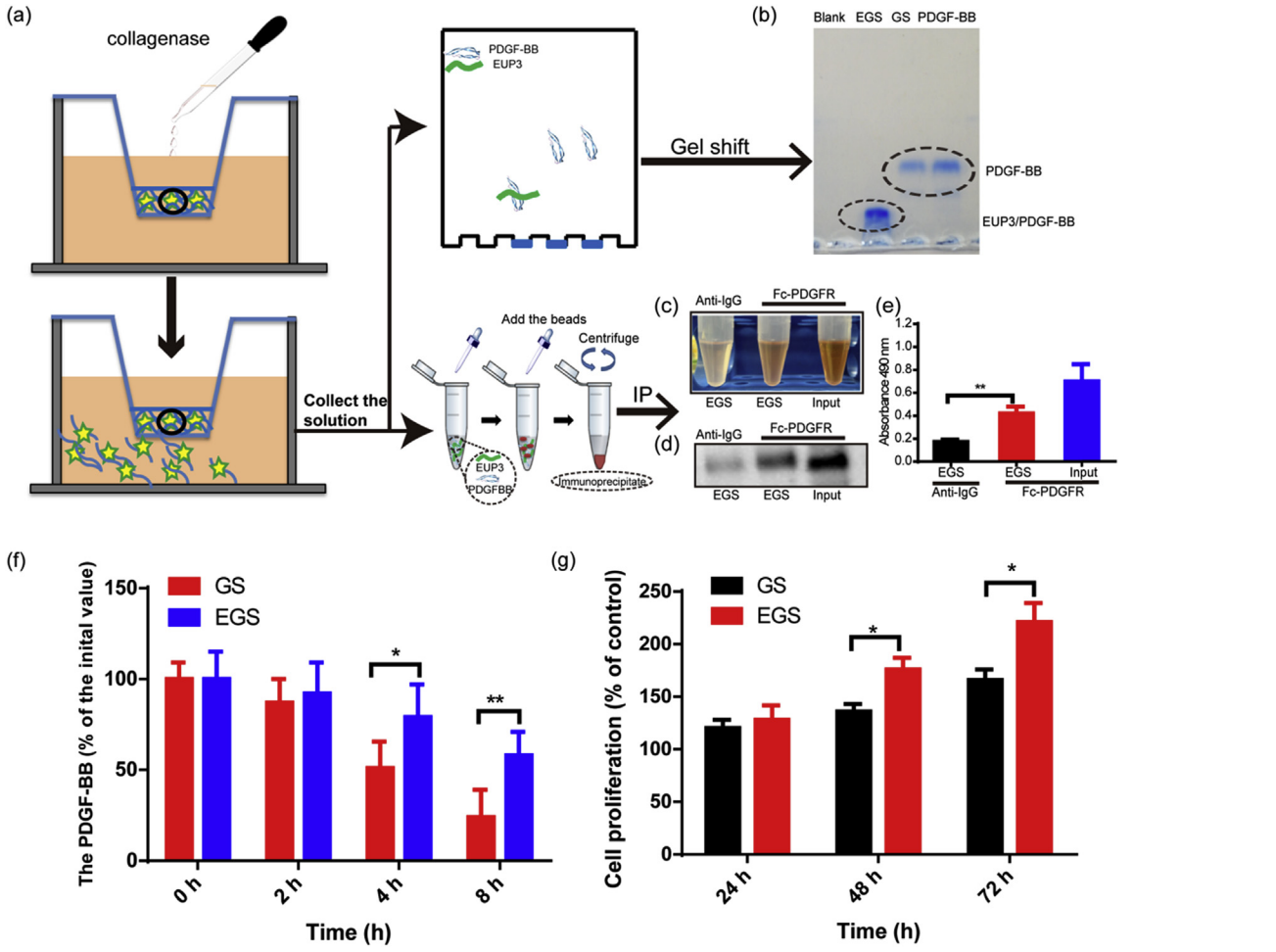

Fig. 4. *In vitro* validation of the PDGF-BB/EUP3 complex released from EGS: a) schematic diagram of the gel-shift and immunoprecipitation assays – GS or EGS samples pre-incubated with PDGF-BB was placed in the upper insert and treated with collagenase, the solution in the lower chambers ('lower-chamber solution') was collected and subjected to further analysis; b) analysis of PDGF-BB in the lower-chamber solution of GS or EGS by gel-shift assay, with recombinant PDGF-BB set as positive control in the rightmost lane; c-e) immunoprecipitation of PDGF-BB from the lower-chamber solution of EGS, followed by c) detection of polysaccharides (EUP3) by sulfuric-phenol assay, d) detection of PDGF-BB by Western blotting and e) quantification of the polysaccharides. In addition, the un-precipitated solution blotted by Fc-PDGFR and the precipitated solution blotted by anti-IgG set as input control and isotype control, respectively; f) assessment of the stability of PDGF-BB released from EGS or GS, to which a commercial maximum recovery diluent was added to mimic the wound environment, followed by determination of PDGF-BB by ELISA; g) the effect of the lower-chamber solution of EGS and GS on fibroblasts proliferation ($^*p < 0.05$).

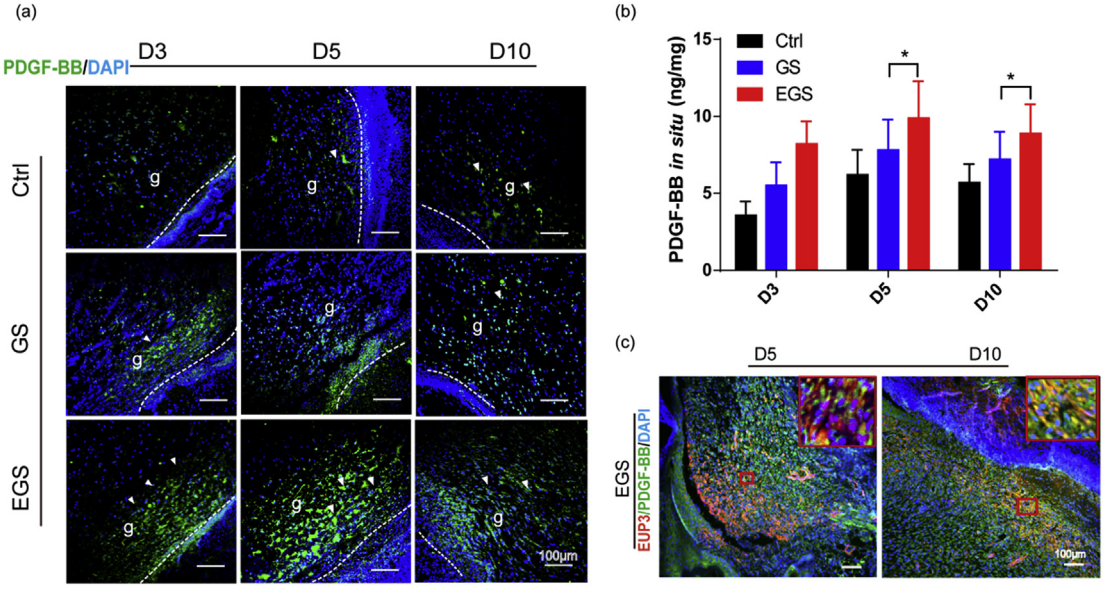

Fig. 5. *In vivo* sequestration of PDGF-BB by EGS: a) IF staining for endogenous PDGF-BB at the site of EGS/GS implantation (g: granulation); b) determination of PDGF-BB content retained in the EGS/GS sponges *in situ* ($^*p < 0.05$); c) observation of the co-localisation of endogenous PDGF-BB and EUP3 *in situ*, in which IF staining was performed for PDGF-BB and EUP3 was fluorescently labelled before implantation.

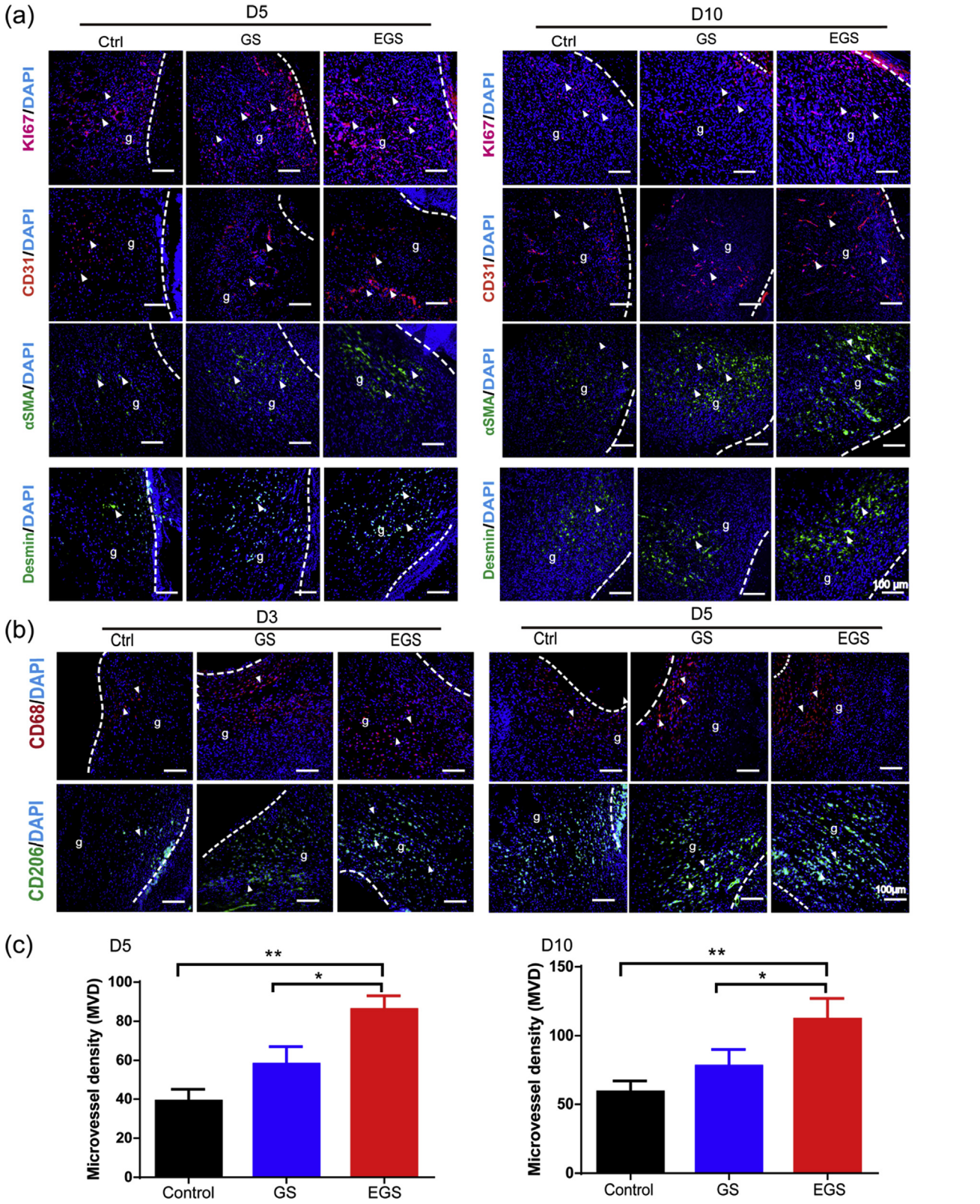

Fig. 6. *In vivo* enhancement of PDGF-BB-mediated cellular activities by EGS: a) IF staining for evaluating cell proliferation (ki67), endothelial cell recruitment (CD31) and vascular maturation (α-SMA and Desmin) in the implanted EGS or GS; b) IF staining for assessing macrophage activities around the implanted sponges, with white arrows indicating accumulated positive signal; c) quantification of the microvascular density at day 5 and 10 ($^{*}p < 0.05$ and $^{**}p < 0.01$).

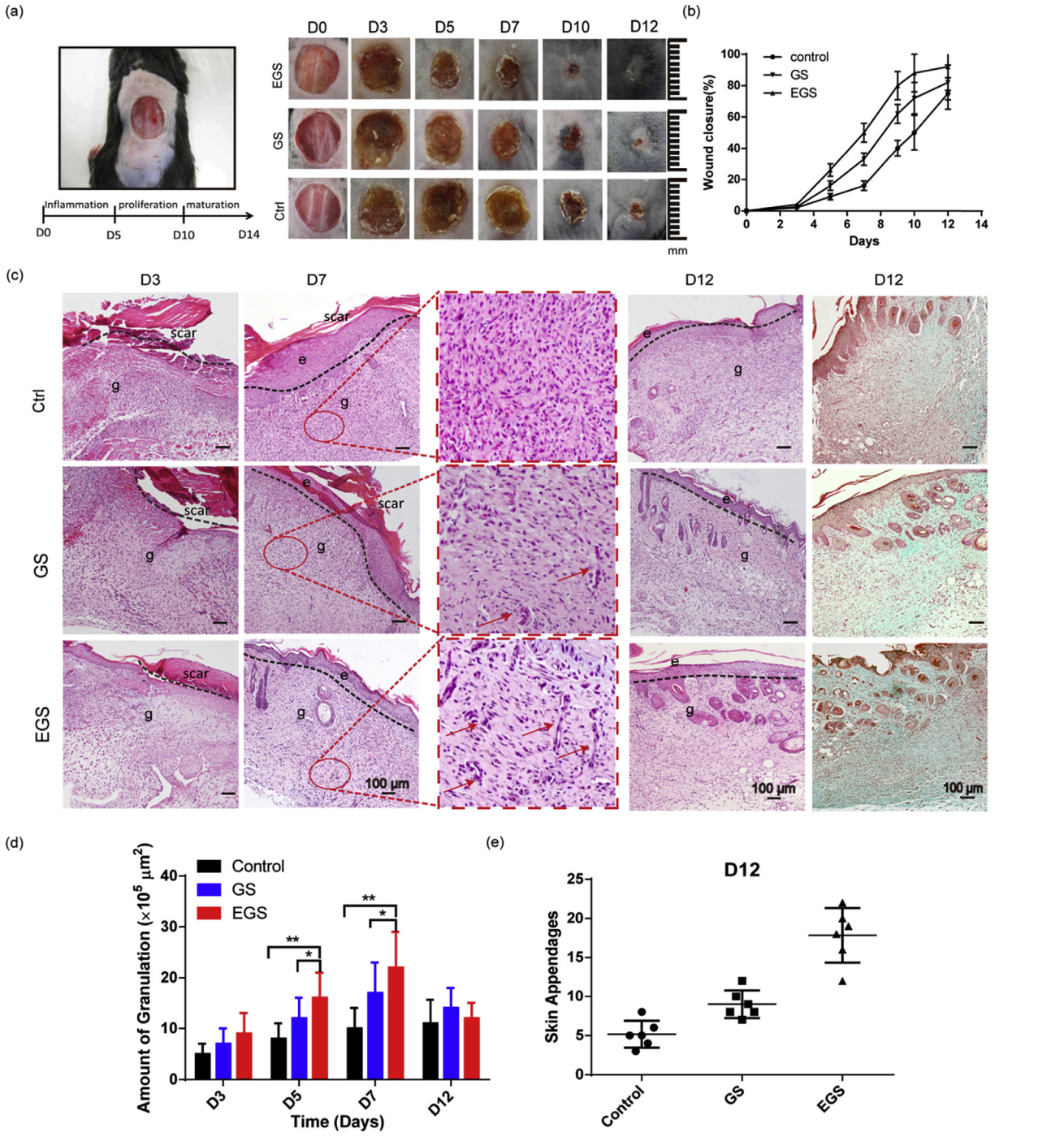

Fig. 7. The efficacy of EGS in enhancing healing of full-thickness wounds created on mice skin: a) gross view of (left) one created wound model and (right) the wounds receiving different treatments; b) the wound closure rate in mice receiving different treatments; c) H&E staining for skin tissues collected from different groups at day 3, day 7 and day 12, and Masson's trichrome staining for the deposition of tissue matrices at the site of injury in different groups at day 12 (red arrows indicate blood vessels; g: granulation, e: epithelium); d) the total granulation area and e) the number of skin appendages at the site of injury in different groups ($^{*}p < 0.05$ and $^{**}p < 0.01$). (For interpretation of the references to colour in this figure legend, the reader is referred to the web version of this article.)

significant differences among the different groups; but from day 5 on, EGS facilitated faster healing than the two other groups. On day 10, the wounds treated with EGS almost completely closed, while uncovered wounds (diameter ~ 4 mm) remained significant in the two other groups. On day 12, all the EGS-treated wounds accomplished healing.

Histological analysis indicated that, at day 3, the granulation tissue appeared in all groups; but at day 7, the epithelisation and vascularisation were accomplished significantly better in EGS-treated wounds than in other groups (Fig. 7c). Particularly, we found increasing numbers of newly blood vessels in EGS (Fig. 7c, red arrows). At day 12, the wounds treated with EGS were completely closed, with faster formation of a continuous, regularly-shaped epithelium, compared with GS or the untreated group (Fig. 7c). We further performed Masson's trichrome staining to examine the deposition of collagen matrices in the wound tissue,

which marked the remodelling of newly formed tissue. In agreement with the H&E staining, the results indicated that newly produced collagen was deposited in the highest amount in the EGS group (Fig. 7c). Quantification of the wound closure indicated that EGS healed the wounds the fastest among the three groups, and the difference was most obvious between day 5 and 7 (Fig. 7d). Interestingly, significantly more skin appendages were found in the neotissue formed in EGS than that in other groups at day 12 (Fig. 7e), suggesting that EGS facilitated healing of the wounds and regenerate more functional tissues. These results highlighted that EGS could induce the formation of tissue microenvironment favourable for neo-tissue growth that led to a both accelerated and improved wound healing.

For any biomaterials to be used *in vivo*, it is important that they exert no (or as little as possible) adverse effect to the body. As reported above, we did not observe death or any abnormal conditions in the animals implanted with EGS throughout the experimental periods. To further confirm that the implants exerted no toxicity, while taking into consideration the release of EUP3, we examined blood coagulation and performed a series of biochemical analyses. First, the PT values of all groups tested at day 3 and day 10 were between 6.8 and 7.2 s and in the normal range, suggesting that blood coagulation was unaffected by EGS implantation (Fig. S7a). Next, the levels of CK (240–300 U/L), LDH (660–700 U/L) and BUN (5.5–6.2 mmol/L) were normal in all groups after 10 days of implantation, excluding the possibility of cardiac or renal toxicity. Meanwhile, the readings of ALT and AST, the two key markers of liver function, remained close among different groups (all between 27 and 31 U/L) (Fig. S7b). Collectively, together with the gross observation of the animal conditions, these analytical data suggested that EGS exerted no adverse responses *in vivo* and highlighted the safety of this natural polymer-based scaffold.

The overall performance of EGS has validated our hypothesis that enriching endogenous GF with an ECM-mimetic biomaterial could be a novel, safe and effective approach to promote tissue regeneration. First, to our knowledge, our design is the first attempt focusing on harnessing the power of endogenous PDGF-BB, in comparison to conventional methods of delivering exogenous GFs or transfecting encoding genes [69,70]. Our design was built upon the physiological mechanism that several GFs are present in elevated levels *in situ* in response to injuries. In sequestering endogenous PDGF-BB, EGS demonstrated the way to creating an 'inductive niche' [1] to activate the endogenous repairing mechanism of the wounded tissue. In this perspective, our strategy adds weight to – and may be combined with – another methodology that employed GAGs to sequester inflammatory cytokines for wound healing [71]. Second, as a biomaterial system, EGS adequately recapitulated both the general physical property (e.g. 3D network and fibrous microstructure) and subtle biological features (e.g. cell adhesion and GF-affinity) of the skin ECM. In accordance with our design, EUP3 and gelatin, the two major components, exhibited their unique PDGF-BB-binding affinity and enzyme-triggered degradation profile, respectively (in tandem with other potential advantages of gelatin in wound healing [72]). Their functions underpinned the 'retention-and-release' effect of EGS that proved fundamental to the accomplishment of tissue regeneration. Third, as a novel polysaccharide molecule, EUP3 has demonstrated great potential for use in the fabrication of bioactive materials. It is easy to be incorporated in fibres and stable under physiological circumstances, and has no such safety concerns that are often found in polysaccharides with potential GF-binding activities, such as those highly-sulphated ones isolated from seaweeds (e.g. carrageenans) [34,35] or derived from animals (e.g. heparin) [31–33]. In addition, its specific affinity for PDGF-BB, which is particularly desirable for skin tissue regeneration, was rarely found in alternative molecules suitable for fabrication of biomaterials.

4. Conclusion

In this study, we report the design of an ECM-mimetic biomaterials sponge (EGS) that successfully accelerated the healing of full-thickness skin wounds in mice. As its most prominent feature, EGS could effectively bind and retain endogenous PDGF-BB *via* the selective affinity of its polysaccharide component for this growth factor. Meanwhile, EGS managed to release PDGF-BB (together with EUP3) in response to the progression of wound healing. In exerting this 'retention-and-release' effect, EGS successfully recapitulated one of the most powerful, distinctive and sought after features of native ECM – *in situ* sequestration of growth factors for regulating tissue development. Our data from serial *in vitro* and *in vivo* examinations showed that EGS efficiently facilitated PDGF-BB-mediated cellular functions that led to an accelerated wound healing with enhanced neovascularisation, controlled immune activation and improved neotissue formation. Notably, no exogenous PDGF-BB – either in the form of recombinant proteins or encoding genes – was delivered in our investigation, and the regeneration was accomplished relying upon the power of endogenous PDGF-BB. Thus, combining its convincing therapeutic performance, optimal physical properties, ECM-mimicking fibrous morphology and demonstrated safety in the mice body, EGS demonstrated the potential to target and activate a specific endogenous mechanism in tissue repair, which may represent a new strategy for the design of regenerative materials.

Acknowledgements

This study was financially supported by the funding grants from Fundo para o Desenvolvimento das Ciências e da Tecnologia, Macau (FDCT 126/2016/A3, 080/2016/A2), the University of Macau (MYRG2016-00031-ICMS-QRCM, and MYRG2015-00160-ICMS-QRCM), the open fund of the State Key Laboratory of Quality Research in Chinese Medicine, University of Macau (No. 005), and National Science Foundation of China (51503232).

Appendix A. Supplementary data

Supplementary data related to this article can be found at https://doi.org/10.1016/j.biomaterials.2017.09.028.

References

[1] S.J. Forbes, N. Rosenthal, Preparing the ground for tissue regeneration: from mechanism to therapy, Nat. Med. 20 (8) (2014) 857–869.
[2] G.C. Gurtner, S. Werner, Y. Barrandon, M.T. Longaker, Wound repair and regeneration, Nature 453 (7193) (2008) 314–321.
[3] P.E. Bourgine, E. Gaudiello, B. Pippenger, C. Jaquiery, T. Klein, S. Pigeot, A. Todorov, S. Feliciano, A. Banfi, I. Martin, Engineered extracellular matrices as biomaterials of tunable composition and function, Adv. Funct. Mater. 27 (7) (2017).
[4] U. Freudenberg, Y.K. Liang, K.L. Kiick, C. Werner, Glycosaminoglycan-based biohybrid hydrogels: a sweet and smart choice for multifunctional biomaterials, Adv. Mater. 28 (40) (2016) 8861–8891.
[5] M.R. Lutolf, F.E. Weber, H.G. Schmoekel, J.C. Schense, T. Kohler, R. Muller, J.A. Hubbell, Repair of bone defects using synthetic mimetics of collagenous extracellular matrices, Nat. Biotechnol. 21 (5) (2003) 513–518.
[6] T.H. Barker, The role of ECM proteins and protein fragments in guiding cell behavior in regenerative medicine, Biomaterials 32 (18) (2011) 4211–4214.
[7] P. Dan, E. Velot, G. Francius, P. Menu, V. Decot, Human-derived extracellular matrix from Wharton's jelly: an untapped substrate to build up a standardized and homogeneous coating for vascular engineering, Acta Biomater. 48 (2017) 227–237.
[8] E.S. Place, N.D. Evans, M.M. Stevens, Complexity in biomaterials for tissue engineering, Nat. Mater. 8 (6) (2009) 457–470.

[9] M.M. Martino, F. Tortelli, M. Mochizuki, S. Traub, D. Ben-David, G.A. Kuhn, R. Muller, E. Livne, S.A. Eming, J.A. Hubbell, Engineering the growth factor microenvironment with fibronectin domains to promote wound and bone tissue healing, Sci. Transl. Med. 3 (100) (2011).

[10] L. Yildirimer, N.T.K. Thanh, A.M. Seifalian, Skin regeneration scaffolds: a multimodal bottom-up approach, Trends Biotechnol. 30 (12) (2012) 638–648.

[11] M.M. Martino, S. Brkic, E. Bovo, M. Burger, D.J. Schaefer, T. Wolff, L. Gürke, P.S. Briquez, H.M. Larsson, R. Gianni-Barrera, J.A. Hubbell, A. Banfi, Extracellular matrix and growth factor engineering for controlled angiogenesis in regenerative medicine, Front. Bioeng. Biotechnol. 3 (45) (2015).

[12] P.S. Briquez, L.E. Clegg, M.M. Martino, F.M. Gabhann, J.A. Hubbell, Design principles for therapeutic angiogenic materials, Nat. Rev. Mater. 1 (2016) 15006.

[13] K. Lee, E.A. Silva, D.J. Mooney, Growth factor delivery-based tissue engineering: general approaches and a review of recent developments, J. R. Soc. Interface 8 (55) (2010) 153.

[14] C. Wang, S. Poon, S. Murali, C.-Y. Koo, T.J. Bell, S.F. Hinkley, H. Yeong, K. Bhakoo, V. Nurcombe, S.M. Cool, Engineering a vascular endothelial growth factor 165-binding heparan sulfate for vascular therapy, Biomaterials 35 (25) (2014) 6776–6786.

[15] K.J. Manton, D.F.M. Leong, S.M. Cool, V. Nurcombe, Disruption of heparan and chondroitin sulfate signaling enhances mesenchymal stem cell-derived osteogenic differentiation via bone morphogenetic protein signaling pathways (vol. 25, pg 2845, 2007), Stem Cells 33 (7) (2015) 2361–2362.

[16] G.A. Hudalla, W.L. Murphy, Biomaterials that regulate growth factor activity via bioinspired interactions, Adv. Funct. Mater. 21 (10) (2011) 1754–1768.

[17] D.G. Belair, W.L. Murphy, Specific VEGF sequestering to biomaterials: influence of serum stability, Acta Biomater. 9 (11) (2013) 8823–8831.

[18] D.H. Yang, D.I. Seo, D.-W. Lee, S.H. Bhang, K. Park, G. Jang, C.H. Kim, H.J. Chun, Preparation and evaluation of visible-light cured glycol chitosan hydrogel dressing containing dual growth factors for accelerated wound healing, J. Ind. Eng. Chem. 53 (2017) 360–370.

[19] C.M. Wang, S. Poon, S. Murali, C.Y. Koo, T.J. Bell, S.F. Hinkley, H.Q. Yeong, K. Bhakoo, V. Nurcombe, S.M. Cool, Engineering a vascular endothelial growth factor 165-binding heparan sulfate for vascular therapy, Biomaterials 35 (25) (2014) 6776–6786.

[20] Z. Liu, R. Yan, A. Al-Salman, Y. Shen, Y. Bu, J. Ma, D.-X. Luo, C. Huang, Y. Jiang, A. Wilber, Y.-Y. Mo, Mei C. Huang, Y. Zhao, D. Cao, Epidermal growth factor induces tumour marker AKR1B10 expression through activator protein-1 signalling in hepatocellular carcinoma cells, Biochem. J. 442 (2) (2012) 273.

[21] S. Mitragotri, P.A. Burke, R. Langer, Overcoming the challenges in administering biopharmaceuticals: formulation and delivery strategies, Nat. Rev. Drug Discov. 13 (9) (2014) 655–672.

[22] T.G. Kim, H. Shin, D.W. Lim, Biomimetic scaffolds for tissue engineering, Adv. Funct. Mater. 22 (12) (2012) 2446–2468.

[23] Q. Li, G. Guo, F. Meng, H.H. Wang, Y. Niu, Q. Zhang, J. Zhang, Y. Wang, L. Dong, C. Wang, A Naturally Derived, Growth factor-binding polysaccharide for therapeutic angiogenesis, ACS Macro Lett. 5 (5) (2016) 617–621.

[24] T.N. Demidova-Rice, M.R. Hamblin, I.M. Herman, Acute and impaired wound healing: pathophysiology and current methods for drug delivery, Part 2: role of growth factors in normal and pathological wound healing: therapeutic potential and methods of delivery, Adv. Skin. Wound Care 25 (8) (2012) 349–370.

[25] M. Belting, M.I. Dorrell, S. Sandgren, E. Aguilar, J. Ahamed, A. Dorfleutner, P. Carmeliet, B.M. Mueller, M. Friedlander, W. Ruf, Regulation of angiogenesis by tissue factor cytoplasmic domain signaling, Nat. Med. 10 (5) (2004) 502–509.

[26] D.M. Brown, S.P. Hong, C.L. Farrell, G.F. Pierce, R.K. Khouri, Platelet-derived growth-factor bb induces functional vascular anastomoses in-vivo, P Natl. Acad. Sci. U. S. A. 92 (13) (1995) 5920–5924.

[27] A. Shibamiya, L. Muhl, S. Tannert-Otto, K.T. Preissner, S.M. Kanse, Nucleic acids potentiate factor VII-activating protease (FSAP)-mediated cleavage of platelet-derived growth factor-BB and inhibition of vascular smooth muscle cell proliferation, Biochem. J. 404 (2007) 45–50.

[28] S. Barrientos, O. Stojadinovic, M.S. Golinko, H. Brem, M. Tomic-Canic, Growth factors and cytokines in wound healing, Wound Repair Regen. 16 (5) (2008) 585–601.

[29] A. Abramsson, S. Kurup, M. Busse, S. Yamada, P. Lindblom, E. Schallmeiner, D. Stenzel, D. Sauvaget, J. Ledin, M. Ringvall, U. Landegren, L. Kjellen, G. Bondjers, J.P. Li, U. Lindahl, D. Spillmann, C. Betsholtz, H. Gerhardt, Defective N-sulfation of heparan sulfate proteoglycans limits PDGF-BB binding and pericyte recruitment in vascular development, Gene Dev. 21 (3) (2007) 316–331.

[30] S. Kurup, A. Abramsson, J.P. Li, U. Lindahl, L. Kjellen, C. Betsholtz, H. Gerhardt, D. Spillmann, Heparan sulphate requirement in platelet-derived growth factor B-mediated pericyte recruitment, Biochem. Soc. T 34 (2006) 454–455.

[31] S.J. Paluck, T.H. Nguyen, H.D. Maynard, Heparin-mimicking polymers: synthesis and biological applications, Biomacromolecules 17 (11) (2016) 3417–3440.

[32] H. Bussey, J.L. Francis, H.C. Grp, Heparin overview and issues, Pharmacotherapy 24 (8) (2004) 103–107.

[33] S. Battistelli, A. Genovese, T. Gori, Heparin-induced thrombocytopenia in surgical patients, Am. J. Surg. 199 (1) (2010) 43–51.

[34] W.I. Chan, G.P. Zhang, X. Li, C.H. Leung, D.L. Ma, L. Dong, C.M. Wang, Carrageenan activates monocytes via type-specific binding with interleukin-8: an implication for design of immuno-active biomaterials, Biomater. Sci-Uk 5 (3) (2017) 403–407.

[35] J.J. Liu, X.D. Zhan, J.B. Wan, Y.T. Wang, C.M. Wang, Review for carrageenan-based pharmaceutical biomaterials: favourable physical features versus adverse biological effects, Carbohydr. Polym. 121 (2015) 27–36.

[36] P.S. Briquez, L.E. Clegg, M.M. Martino, F.M. Gabhann, J.A. Hubbell, Des. Princ. Ther. angiogenic Mater. 1 (2016) 15006.

[37] S.-M. Lien, L.-Y. Ko, T.-J. Huang, Effect of pore size on ECM secretion and cell growth in gelatin scaffold for articular cartilage tissue engineering, Acta Biomater. 5 (2) (2009) 670–679.

[38] K. Su, C.M. Wang, Recent advances in the use of gelatin in biomedical research, Biotechnol. Lett. 37 (11) (2015) 2139–2145.

[39] J.L. Seltzer, K.T. Akers, H. Weingarten, G.A. Grant, D.W. McCourt, A.Z. Eisen, Cleavage specificity of human skin type IV collagenase (gelatinase). Identification of cleavage sites in type I gelatin, with confirmation using synthetic peptides, J. Biol. Chem. 265 (33) (1990) 20409–20413.

[40] K.N. Riley, I.M. Herman, Collagenase promotes the cellular responses to injury and wound healing in vivo, J. Burns Wounds 4 (2005) e8.

[41] G. Kratz, K. Jansson, M. Gidlund, A. Haegerstrand, Keratinocyte conditioned medium stimulates type IV collagenase synthesis in cultured human keratinocytes and fibroblasts, Brit J. Dermatol. 133 (6) (1995) 842–846.

[42] K.Y. Lee, L. Jeong, Y.O. Kang, S.J. Lee, W.H. Park, Electrospinning of polysaccharides for regenerative medicine, Adv. Drug Deliv. Rev. 61 (12) (2009) 1020–1032.

[43] J.R. Dias, P.L. Granja, P.J. Bartolo, Advances in electrospun skin substitutes, Prog. Mater. Sci. 84 (2016) 314–334.

[44] S.S. Sreedhara, N.R. Tata, A novel method for measurement of porosity in nanofiber mat using pycnometer in filtration, J. Eng. Fiber Fabr. 8 (2013) 132–137.

[45] T. Zuo, N. Zhang, Q. Zhang, H. Shi, S. Lu, C. Xue, Q.-J. Tang, Transportation of squid ink polysaccharide SIP through intestinal epithelial cells and its utilization in the gastrointestinal tract, J. Funct. Foods 22 (2016) 408–416.

[46] Z. Wang, C. Wang, S. Liu, W. He, L. Wang, J. Gan, Z. Huang, Z. Wang, H. Wei, J. Zhang, L. Dong, Specifically formed corona on silica nanoparticles enhances transforming growth factor β1 activity in triggering lung fibrosis, ACS Nano 11 (2) (2017) 1659–1672.

[47] J. Said, C.C. Dodoo, M. Walker, D. Parsons, P. Stapleton, A.E. Beezer, S. Gaisford, An in vitro test of the efficacy of silver-containing wound dressings against Staphylococcus aureus and Pseudomonas aeruginosa in simulated wound fluid, Int. J. Pharm. 462 (1) (2014) 123–128.

[48] S.J. Lee, Y.-H. Shim, J.-S. Oh, Y.-I. Jeong, I.-K. Park, H.C. Lee, Folic-acid-conjugated pullulan/poly(DL-lactide-co-glycolide) graft copolymer nanoparticles for folate-receptor-mediated drug delivery, Nanoscale Res. Lett. 10 (1) (2015) 43.

[49] A.C. Mitchell, P.S. Briquez, J.A. Hubbell, J.R. Cochran, Engineering growth factors for regenerative medicine applications, Acta Biomater. 30 (2016) 1–12.

[50] S. Murali, B. Rai, C. Dombrowski, J.L.J. Lee, Z.X.H. Lim, D.S. Bramono, L. Ling, T. Bell, S. Hinkley, S.S. Nathan, J.H. Hui, H.K. Wong, V. Nurcombe, S.M. Cool, Affinity-selected heparan sulfate for bone repair, Biomaterials 34 (22) (2013) 5594–5605.

[51] S.S. Cai, Y.C. Liu, X.Z. Shu, G.D. Prestwich, Injectable glycosaminoglycan hydrogels for controlled release of human basic fibroblast growth factor, Biomaterials 26 (30) (2005) 6054–6067.

[52] D. Park, H. Mewhort, G. Teng, D. Belke, J. Turnbull, D. Svystonyuk, D. Guzzardi, S. Kang, P.W.M. Fedak, Heparin augmentation enhances bioactive properties of acellular extracellular matrix scaffold, Tissue Eng. Part A (2017), https://doi.org/10.1089/ten.tea.2017.0004.

[53] B. Rai, V. Nurcombe, S.M. Cool, Heparan sulfate-based treatments for regenerative medicine, Crit. Rev. Eukar Gene 21 (1) (2011) 1–12.

[54] S. Suvarna, B. Espinasse, R. Qi, R. Lubica, M. Poncz, D.B. Cines, M.R. Wiesner, G.M. Arepally, Determinants of PF4/heparin immunogenicity, Blood 110 (13) (2007) 4253–4260.

[55] S. Ashikari-Hada, H. Habuchi, Y. Kariya, N. Itoh, A.H. Reddi, K. Kimata, Characterization of growth factor-binding structures in heparin/heparan sulfate using an octasaccharide library, J. Biol. Chem. 279 (13) (2004) 12346–12354.

[56] J. Liu, R.J. Linhardt, Chemoenzymatic synthesis of heparan sulfate and heparin, Nat. Prod. Rep. 31 (12) (2014) 1676–1685.

[57] B. Gharibi, M.S. Ghuman, F.J. Hughes, Akt- and Erk-mediated regulation of proliferation and differentiation during PDGFRβ-induced MSC self-renewal, J. Cell. Mol. Med. 16 (11) (2012) 2789–2801.

[58] A. Tokunaga, T. Oya, Y. Ishii, H. Motomura, C. Nakamura, S. Ishizawa, T. Fujimori, Y. Nabeshima, A. Umezawa, M. Kanamori, T. Kimura, M. Sasahara, PDGF receptor beta is a potent regulator of mesenchymal stromal cell function, J. Bone Min. Res. 23 (9) (2008) 1519–1528.

[59] A. Armulik, G. Genové, C. Betsholtz, Pericytes: developmental, physiological, and pathological perspectives, problems, and promises, Dev. Cell 21 (2) (2011) 193–215.

[60] R. Gianni-Barrera, M. Bartolomeo, B. Vollmar, V. Djonov, A. Banfi, Split for the cure: VEGF, PDGF-BB and intussusception in therapeutic angiogenesis, Biochem. Soc. T 42 (2014) 1637–1642.

[61] I. Helfrich, D. Schadendorf, Blood vessel maturation, vascular phenotype and angiogenic potential in malignant melanoma: one step forward for overcoming anti-angiogenic drug resistance? Mol. Oncol. 5 (2) (2011) 137–149.

[62] T.F. Deuel, R.M. Senior, J.S. Huang, G.L. Griffin, Chemotaxis of monocytes and neutrophils to platelet-derived growth factor, J. Clin. Investig. 69 (4) (1982)

1046–1049.
[63] J.S. Cho, T.C. Fang, T.L. Reynolds, D.J. Sofia, S. Hamann, L.C. Burkly, PDGF-BB promotes type I IFN-dependent vascular alterations and monocyte recruitment in a model of dermal fibrosis, Plos One 11 (9) (2016).
[64] K.L. Spiller, R.R. Anfang, K.J. Spiller, J. Ng, K.R. Nakazawa, J.W. Daulton, G. Vunjak-Noyakovic, The role of macrophage phenotype in vascularization of tissue engineering scaffolds, Biomaterials 35 (15) (2014) 4477–4488.
[65] Y.X. Feng, Q. Li, D. Wu, Y.M. Niu, C. Yang, L. Dong, C.M. Wang, A macrophage-activating, injectable hydrogel to sequester endogenous growth factors for in situ angiogenesis, Biomaterials 134 (2017) 128–142.
[66] J. Yang, X. Liu, S.B. Nyland, R.R. Zhang, L.K. Ryland, K. Broeg, K.T. Baab, N.R. Jarbadan, R. Irby, T.P. Loughran, Platelet-derived growth factor mediates survival of leukemic large granular lymphocytes via an autocrine regulatory pathway, Blood 115 (1) (2010) 51–60.
[67] Y.L. Yang, P. Andersson, K. Hosaka, Y. Zhang, R.H. Cao, H. Iwamoto, X.J. Yang, M. Nakamura, J. Wang, R.J. Zhuang, H. Morikawa, Y. Xue, H. Braun, R. Beyaert, N. Samani, S. Nakae, E. Hams, S. Dissing, P.G. Fallon, R. Langer, Y.H. Cao, The PDGF-BB-SOX7 axis-modulated IL-33 in pericytes and stromal cells promotes metastasis through tumour-associated macrophages, Nat. Commun. 7 (2016).
[68] K.S. Torok, K. Kurzinski, C. Kelsey, J. Yabes, K. Magee, A.N. Vallejo, T. Medsger, C.A. Feghali-Bostwick, Peripheral blood cytokine and chemokine profiles in juvenile localized scleroderma: T-helper cell-associated cytokine profiles, Semin. Arthritis Rheu. 45 (3) (2015) 284–293.
[69] N. Zilony, M. Rosenberg, L. Holtzman, H. Schori, O. Shefi, E. Segal, Prolonged controlled delivery of nerve growth factor using porous silicon nanostructures, J. Control. Release 257 (2017) 51–59.
[70] L.K. Branski, C.T. Pereira, D.N. Herndon, M.G. Jeschke, Gene therapy in wound healing: present status and future directions, Gene Ther. 14 (1) (2006) 1–10.
[71] N. Lohmann, L. Schirmer, P. Atallah, E. Wandel, R.A. Ferrer, C. Werner, J.C. Simon, S. Franz, U. Freudenberg, Glycosaminoglycan-based hydrogels capture inflammatory chemokines and rescue defective wound healing in mice, Sci. Transl. Med. 9 (386) (2017), eaai9044.
[72] B. Cullen, R. Smith, E. Mcculloch, D. Silcock, L. Morrison, Mechanism of action of PROMOGRAN, a protease modulating matrix, for the treatment of diabetic foot ulcers, Wound Repair Regen. 10 (1) (2002) 16–25.